

# Bootstrap Dynamic-Aware 3D Visual Representation for Scalable Robot Learning

Qiwei Liang<sup>1,2,\*</sup> Boyang Cai<sup>2,\*</sup> Minghao Lai<sup>2,\*</sup> Sitong Zhuang<sup>2,\*</sup>  
 Tao Lin<sup>4</sup> Yan Qin<sup>2</sup> Yixuan Ye<sup>5</sup> Jiaming Liang<sup>2</sup> Renjing Xu<sup>1,†</sup>

<sup>1</sup>Hong Kong University of Science and Technology (Guangzhou) <sup>2</sup>Shenzhen University

<sup>3</sup>Beijing Jiaotong University <sup>4</sup>Central South University

\*Equal contribution †Corresponding author

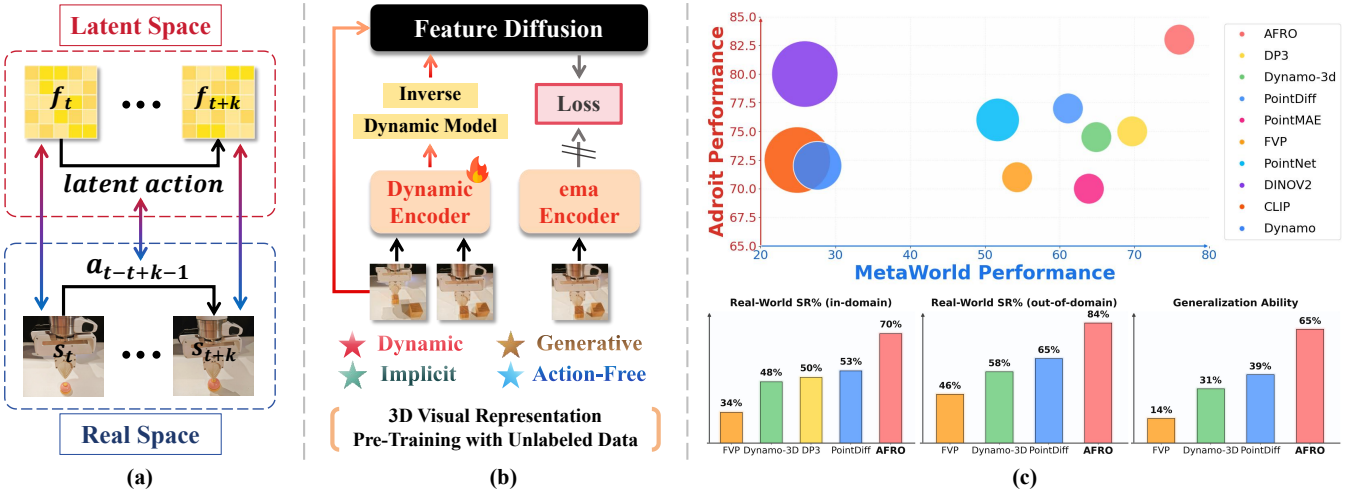


Figure 1. (a) The relationship between robot manipulation in real space and its abstraction in latent space. (b) Our framework learns dynamics-aware 3D visual features in latent space, replacing static representations without relying on explicit action labels or reconstruction. (c) AFRO achieves higher success rates and stronger generalization than baseline methods in both simulation and real-world tasks.

## Abstract

Despite strong results on recognition and segmentation, current 3D visual pre-training methods often underperform on robotic manipulation. We attribute this gap to two factors: the lack of state-action-state dynamics modeling and the unnecessary redundancy of explicit geometric reconstruction. We introduce **AFRO**, a self-supervised framework that learns dynamics-aware 3D representations without action or reconstruction supervision. **AFRO** casts state prediction as a generative diffusion process and jointly models forward and inverse dynamics in a shared latent space to capture causal transition structure. To prevent feature leakage in action learning, we employ feature differencing and inverse-consistency supervision, improving the quality and stability of visual features. When combined with Diffusion Policy, **AFRO** substantially increases manipulation success rates across 16 simulated and 4 real-world tasks, outperforming existing pre-training approaches. The framework also scales favorably with data volume and task complexity. Qualitative visualizations indicate that **AFRO** learns semantically rich,

discriminative features, offering an effective pre-training solution for 3D representation learning in robotics. Project page: <https://kolakivy.github.io/AFRO/>

## 1. Introduction

Visual pre-training has significantly advanced robotic manipulation by decoupling representation learning from policy learning: Models acquire general visual priors from large-scale datasets before transferring them to downstream control tasks [9, 19, 20, 36, 37, 40, 55]. This paradigm enables richer feature learning and facilitates cross-domain transfer. Recent 2D approaches (e.g., MVP [49], R3M [27], VIP [26]) leverage large-scale image or video corpora for training and have substantially improved manipulation performance.

However, while 3D point clouds inputs offer more geometric information for better efficiency and generalization [14, 25, 65], 3D visual pre-training for robotic manipulation remains underexplored; meanwhile, standardized pipelines and generative tools are rapidly expanding 3D data

quality and scale. [11, 46]. These trends motivate a central question: *Can we design a scalable 3D visual pre-training framework specially tailored to robotic manipulation?*

Point clouds offer a natural format for 3D data, yet their irregular structure, sparsity, and permutation invariance complicate spatial reasoning and semantic abstraction [33]. Although many 3D pre-training methods have effectively overcome these challenges and demonstrate strong performance on tasks such as object recognition [17, 57] and segmentation [50], they still exhibit suboptimal transfer to robotic manipulation, and even lagging behind 2D foundation models in manipulation benchmarks [18]. We identify that current 3D pre-training approaches overlook two critical aspects:

**Lack of dynamics awareness.** Robotic manipulation is inherently sequential, where each action brings about deliberate changes in the state. However, most existing 3D pre-training frameworks use supervision signals derived solely from the same frame as their inputs. This design overlooks the temporal continuity and causal dependencies underlying state transitions, resulting in a representation space that lacks coherent temporal structure and fails to capture dynamic or causal relationships across states.

**Lack of manipulation-relevant abstraction.** While many 3D pre-training approaches focus on holistic scene reconstruction, they often capture background details irrelevant to control [4]. However, incorporating such dense representations can mislead policy networks, as they may divert attention from task-critical elements. In contrast, effective manipulation necessitates abstractions that prioritize actionable object regions and interaction dynamics, rather than striving for full-scene fidelity.

Robotic manipulation unfolds as state-action-state trajectories rich in supervisory signal. Yet scalable, task-general visual representation learning often omits these labels, creating a tension: how can a model internalize dynamics without explicit action or transition annotations? We posit that dynamics can emerge through latent-space objectives. Recent advances in latent-predictive learning (e.g., V-JEPA 2 [2]) show that aligning high-level features without pixel-level reconstruction yields broadly generalizable representations. Building on this insight, we introduce AFRO, a self-supervised 3D pre-training framework that learns dynamic-aware, manipulation-relevant representations from point clouds. AFRO aims to (i) learn dynamic-aware representations to model the spatiotemporal relationships across states, and (ii) acquire manipulation-relevant abstractions without explicit reconstruction.

Concretely, AFRO integrates inverse and forward dynamics models (IDM/FDM) to encode state-action-state transitions directly in a latent space. As shown in Figure 1, consecutive point clouds are encoded into feature vectors; the IDM infers a latent action from current and subsequent features, while the FDM predicts the next features given the current features and the inferred latent action. State prediction is performed entirely in the feature space, where the online encoder is trained using a VICReg [3] loss against an expo-

nential moving average(ema) target encoder. To handle multimodal future outcomes, we formulate feature prediction as a diffusion-based generation process that encourages upstream modules to supply informative conditions. Through this dynamics-driven learning, the feature encoder is guided to attend to regions with motion changes, thereby encoding representations that are more relevant to manipulation.

To prevent latent action shortcircuiting and feature leakage in IDM learning, we input feature differences instead of raw feature pairs, forcing the model to reason over action-driven change rather than memorize states. We further introduce inverse-consistency supervision: the same pipeline is applied in reverse to explain previous states from future observations. By requiring the latent action to account for both forward prediction and backward explanation, we curb degenerate solutions and stabilize representation learning.

We evaluate AFRO on 16 simulated and 4 real-world manipulation tasks spanning diverse skills (e.g., sliding, pressing, pushing). Across benchmarks, AFRO consistently outperforms strong 2D/3D pretraining baselines and imitation-from-scratch, with advantages that scale with both data volume and domain diversity. Pretraining on the large-scale RH20T [11] dataset further strengthens downstream results, yielding robust gains across all tasks.

Our core contributions are: (1) We propose a 3D visual pretraining framework for robotic manipulation that learns dynamics-aware representations directly in latent space, modeling future state uncertainties with a generative diffusion process while avoiding explicit reconstruction. (2) To our knowledge, we are the first to introduce latent actions into 3D visual learning, and design feature-differencing and inverse-consistency supervision to prevent shortcut learning and feature leakage, thereby enhancing representation quality and stability. (3) Extensive simulation and real-robot experiments show that our method outperforms a range of advanced competing baselines; visualizations and ablations further validate the contribution of each component.

## 2. Related Work

### 2.1. Visual Pretraining for Robot Manipulation

Visual pretraining significantly enhances data efficiency in robotic manipulation by learning transferable representations from large-scale visual data [10, 52]. Early 2D approaches such as R3M [27], MVP [49], and VIP [26] leverage contrastive or masked modeling techniques to extract semantic pixel-level features from images. However, these methods are confined to image-space reasoning and lack explicit 3D geometric awareness, which is a crucial aspect for accurately perceiving spatial in real-world environments.

Recent work has thus shifted toward 3D visual pre-training to better capture scene geometry. For instance, 3D-MVP [34] extends MVP by incorporating multi-view masked autoencoding on large-scale 3D data; SUGAR [5] jointly learns semantic and affordance representations from point clouds, thereby improving zero-shot manipulation ca-

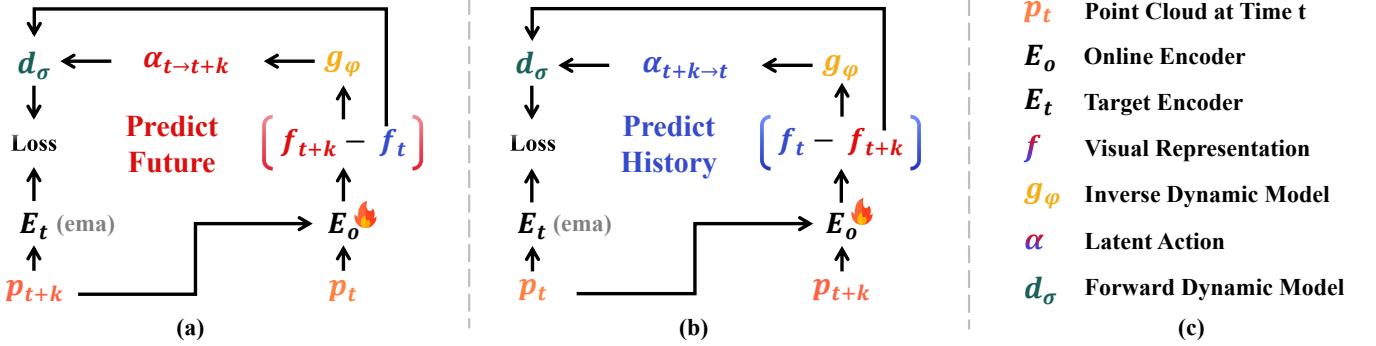


Figure 2. Overall framework of our method. **(a)** Predict Future: Given point clouds  $\mathcal{P}_t$  and  $\mathcal{P}_{t+k}$ , the online encoder  $f_\phi$  encodes both to obtain  $\mathbf{z}_t$  and  $\mathbf{z}_{t+k}$ . The inverse dynamics model  $g_\psi$  takes the difference  $(\mathbf{z}_{t+k} - \mathbf{z}_t)$  to infer the forward latent action  $\alpha_{t \rightarrow t+k}$ . The target encoder  $f_\xi$  (EMA-updated) encodes only  $\mathcal{P}_{t+k}$  to yield the teacher target  $\tilde{\mathbf{z}}_{t+k}$ . The forward dynamics model  $h_\theta$  predicts the future feature by mapping  $(\mathbf{z}_t, \alpha_{t \rightarrow t+k}) \mapsto \hat{\mathbf{z}}_{t+k}$  and aligning it to  $\tilde{\mathbf{z}}_{t+k}$ , which explicitly drives  $f_\phi$  to learn dynamics-aware representations. **(b)** Predict History: Different from (a), using the difference  $(\mathbf{z}_t - \mathbf{z}_{t+k})$ ,  $g_\psi$  infers the backward latent action  $\alpha_{t+k \rightarrow t}$ ;  $f_\xi$  encodes only  $\mathcal{P}_t$  to obtain  $\tilde{\mathbf{z}}_t$ ; then  $h_\theta$  maps  $(\mathbf{z}_{t+k}, \alpha_{t+k \rightarrow t}) \mapsto \hat{\mathbf{z}}_t$  and aligns it with  $\tilde{\mathbf{z}}_t$ . Other steps are symmetric to (a) and omitted for brevity. **(c)** Notation Summary:  $\mathcal{P}_t$  point cloud;  $f_\phi$  online encoder;  $f_\xi$  target encoder;  $\mathbf{z}$  student feature;  $\tilde{\mathbf{z}}$  teacher feature;  $g_\psi$  inverse dynamics model;  $\alpha$  latent action;  $h_\theta$  forward dynamics model.

pabilities. However, most existing 3D methods still overlook the inherent temporal dynamics that characterize robotic manipulation. Although FVP [15] advances this direction with diffusion-based future prediction, it remains dependent on explicit scene reconstruction. In contrast, our approach AFRO introduces action-free 3D pretraining that learns dynamic-aware representations directly in latent space, effectively bridging 3D perception and embodied behavior without relying on action labels or reconstruction.

## 2.2. Latent Actions for Robot Learning

Latent actions encode state transitions into low-dimensional variables, providing an alternative to expensive action annotations. [1, 12, 23, 28, 60] Early methods used inverse dynamics models (IDM) for pretraining, while later approaches jointly learned IDM and forward dynamics models (FDM) in visual spaces to improve sample efficiency. [6, 8, 21, 41] Current research falls into three categories: **(1)** Using latent actions as policy supervision from unlabeled videos, as in CLAM [24] and CoMo [53]; **(2)** Vision-language-action pretraining—e.g., LAPA [54] discretizes frame changes into tokens for efficient regression, and UniVLA [4] learns task-centric latent actions in DINO space for cross-embodiment generalization; **(3)** Reinforcement learning with constrained action spaces to address OOD issues, as in PLAS [64].

Recently, Dynamo [30] leverages latent actions in visual pretraining to capture dynamic changes in manipulation, enabling it to achieve strong performance transfer on downstream tasks. However, these methods remain confined to 2D visual spaces. We adapt latent actions to 3D pretraining and mitigate IDM’s tendency to overfit future features by: (i) using feature differencing rather than frame stacking as IDM input, and (ii) introducing inverse-consistency supervision, whereby inverse latent actions are constructed to enable the FDM to predict historical states from future ones, thereby improving reversibility and temporal consistency.

## 3. Preliminary

We aim to learn dynamics-aware 3D representations from unlabeled point cloud demonstrations. Our approach builds on a latent dynamics modeling paradigm, consisting of an online visual encoder  $f_\phi$ , an inverse dynamics model (IDM)  $g_\psi$ , and a forward dynamics model (FDM)  $h_\theta$ . Given consecutive point clouds  $\mathcal{P}_t$  and  $\mathcal{P}_{t+k}$ , the encoder first extracts their features  $\mathbf{z}_t$  and  $\mathbf{z}_{t+k}$ . The IDM then infers a latent action that explains the transition:

$$\alpha_{t \rightarrow t+k} = g_\psi(\mathbf{z}_t, \mathbf{z}_{t+k}), \quad (1)$$

which is intended to capture the underlying motion. The FDM uses this action to predict the future feature:

$$\hat{\mathbf{z}}_{t+k} = h_\theta(\mathbf{z}_t, \alpha_{t \rightarrow t+k}), \quad (2)$$

enabling state prediction entirely in the latent space. An EMA-updated target encoder  $f_\xi$  provides stable regression targets  $\tilde{\mathbf{z}}$ , avoiding explicit reconstruction.

While this framework offers a principled starting point, we identify two critical limitations in its naive implementation. First, the IDM is prone to *feature leakage* instead of learning meaningful transitions, as it may exploit shortcuts by directly encoding information from  $\mathbf{z}_{t+k}$ , leading to degenerate latent actions that fail to represent dynamics. Second, standard FDMs are typically deterministic and struggle to capture the *multimodal uncertainty* of real-world interactions, often predicting averaged, unrealistic futures.

To overcome these issues, we introduce two core innovations in Sec. 4:

1. A **feature-differencing and reverse consistency** framework for latent action learning, which prevents feature leakage and enhances temporal coherence (Sec. 4.1).
2. A **diffusion-based forward dynamics model** that captures multimodal future distributions, enabling robust and diverse state prediction (Sec. 4.2).

### Inverse Dynamic Model

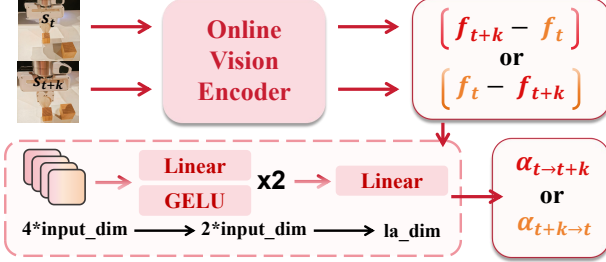


Figure 3. Given the differential feature  $(\mathbf{z}_{t+k} - \mathbf{z}_t)$  or  $(\mathbf{z}_t - \mathbf{z}_{t+k})$ , the inverse dynamics model  $g_\psi$  passes it through two stacked Linear–GELU layers followed by a final Linear projection to produce the latent action  $\alpha_{t+k}$  or  $\alpha_{t+k-t}$ , which encodes the implicit motion between consecutive states.

## 4. Method

**Overview.** As shown in Fig. 2, our framework learns 3D dynamics-aware representations from unlabeled point cloud sequences without reconstruction. It includes three parts: Sec. 4.1 introduces latent action modeling, Sec. 4.2 presents the diffusion-based forward dynamics, and Sec. 4.3 describes the representation matching objective.

### 4.1. Latent Action Modeling

Naively training inverse and forward dynamics on consecutive features  $\mathbf{z}_t$  and  $\mathbf{z}_{t+k}$  often causes feature leakage. Without explicit action supervision, the inverse model can reduce its loss by implicitly copying information from  $\mathbf{z}_{t+k}$  instead of reasoning about how the system transitioned between states. This shortcut undermines temporal reasoning, prevents the model from discovering meaningful dynamics, and ultimately produces degenerate latent actions.

We therefore model *changes* in representation rather than the representations themselves. Concretely, instead of feeding both  $\mathbf{z}_t$  and  $\mathbf{z}_{t+k}$  into the inverse model, we take their difference and learn latent actions directly from the displacement:

$$\alpha_{t+k} = g_\psi(\mathbf{z}_{t+k} - \mathbf{z}_t), \quad (3)$$

where  $g_\psi$  is a lightweight MLP that maps the feature difference into a compact latent action space. This differential view emphasizes what changed and de-emphasizes what stayed the same, naturally filtering out static scene content and highlighting motion-relevant cues. In practice, we find this simple choice stabilizes training and makes the learned actions easier to interpret.

Beyond differencing, we also introduce an **inverse-consistency supervision** to promote temporal coherence. We define the inverse mapping symmetrically as

$$\alpha_{t+k-t} = g_\psi(\mathbf{z}_t - \mathbf{z}_{t+k}), \quad (4)$$

encouraging the model to learn transformations that are approximately reversible and physically plausible. The forward dynamics model  $h_\theta$  is then asked to reconstruct the

### Forward Dynamic Model

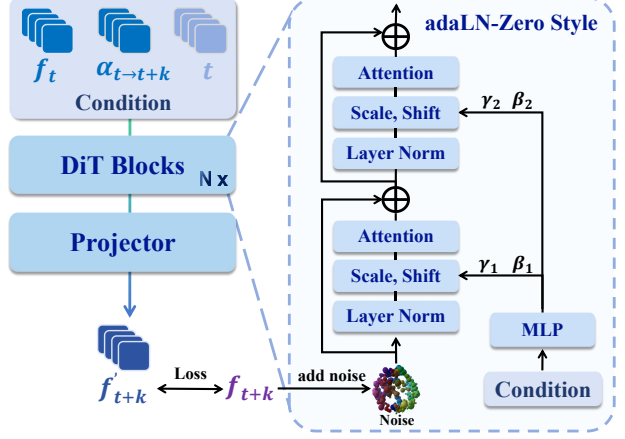


Figure 4. Architecture of the Forward Dynamic Model. An AdaLN-Zero diffusion transformer  $h_\theta$  conditions on  $\mathbf{z}_t$ , latent action  $\alpha_{t+k}$ , and timestep  $\tau$  encoded via MLPs and concatenation, which modulate LayerNorm through adaptive scale–shift. Attention and projector modules then denoise the latent to reconstruct the future representation  $\hat{\mathbf{z}}_{t+k}$ .

current representation from the future one:

$$\hat{\mathbf{z}}_t = h_\theta(\mathbf{z}_{t+k}, \alpha_{t+k}), \quad (5)$$

which aligns the two directions conceptually and constrains latent actions to be causally consistent. Taken together, differencing plus inverse-consistency provides a lightweight but effective recipe for learning latent actions without explicit labels.

### 4.2. Forward Dynamics with Diffusion Transformer

The future is inherently uncertain and often multimodal, as occlusions and stochastic interactions give rise to many plausible outcomes. Conventional MLP- or transformer-based predictors struggle to capture such uncertainty and tend to average over multiple modes. Instead, we formulate forward prediction as a conditional denoising process: given the current feature  $\mathbf{z}_t$ , the latent action  $\alpha_{t+k}$ , and the diffusion step  $\tau$ , the forward dynamics model  $h_\theta$ —implemented as a diffusion transformer [32] (DiT) with AdaLN-Zero conditioning—maps a noisy sample along with these conditioning signals to a clean future latent representation.

**Noising (forward process).** We corrupt the clean future feature with a standard diffusion forward process:

$$\mathbf{z}_{t+k}^{(\tau)} = \sqrt{\bar{\alpha}_\tau} \mathbf{z}_{t+k} + \sqrt{1 - \bar{\alpha}_\tau} \epsilon, \quad \epsilon \sim \mathcal{N}(\mathbf{0}, \mathbf{I}), \quad (6)$$

where  $\bar{\alpha}_\tau \in (0, 1]$  is the cumulative signal weight (equivalently  $\text{SNR}(\tau) = \bar{\alpha}_\tau / (1 - \bar{\alpha}_\tau)$ ).

**Direct denoising (student).** At training and inference, we take the noisy future feature and produce the clean target in a single pass:

$$\hat{\mathbf{z}}_{t+k} = h_\theta(\mathbf{z}_{t+k}^{(\tau)}, \mathbf{z}_t, \alpha_{t+k}, \tau), \quad (7)$$

Table 1. **Quantitative comparison on simulation benchmarks.** *Type* denotes the pretraining category: **2D-LT** = large-scale 2D pretraining; **3D-LT** = large-scale 3D pretraining; **3D-Pre-S** = static 3D pretraining without dynamic modeling; **3D-Pre-D** = dynamic-aware 3D pretraining with temporal modeling; Input Type: **RGB** = image input; **PC** = point cloud input. **Conclusion:** AFRO achieves the highest success rate across all task categories, demonstrating that our pre-training method can substantially enhance the performance in robot manipulation.

| Method             | Type            | Input Type | MetaWorld   |             |             |               | Adroit                    |             |             |                           |
|--------------------|-----------------|------------|-------------|-------------|-------------|---------------|---------------------------|-------------|-------------|---------------------------|
|                    |                 |            | Easy (3)    | Medium (6)  | Hard (2)    | Very Hard (3) | Mean S.R.                 | Door        | Pen         | Mean S.R.                 |
| CLIP [35]          | 2D-LT           | RGB        | 29.3        | 14.0        | 5.0         | 55.3          | 24.9 ( $\downarrow$ 51.1) | 61.0        | 84.0        | 72.5 ( $\downarrow$ 10.5) |
| DINOv2 [29]        | 2D-LT           | RGB        | 34.0        | 14.0        | 5.0         | 55.3          | 25.9 ( $\downarrow$ 50.1) | 76.0        | 84.0        | 80.0 ( $\downarrow$ 3.0)  |
| PointNet [33]      | 3D-LT           | PC         | 71.3        | 49.7        | 23.0        | 55.3          | 51.7 ( $\downarrow$ 24.3) | 80.0        | 72.0        | 76.0 ( $\downarrow$ 7.0)  |
| PointMAE [31]      | 3D-Pre-S        | PC         | 77.3        | 61.3        | 42.0        | 70.0          | 63.9 ( $\downarrow$ 12.1) | 64.0        | 76.0        | 70.0 ( $\downarrow$ 13.0) |
| PointDif [61]      | 3D-Pre-S        | PC         | 83.3        | 58.0        | 41.0        | 58.7          | 61.1 ( $\downarrow$ 14.9) | 76.0        | 78.0        | 77.0 ( $\downarrow$ 6.0)  |
| DynaMo [30]        | 2D-Pre-D        | RGB        | 42.0        | 21.7        | 14.0        | 34.0          | 27.6 ( $\downarrow$ 48.4) | 76.0        | 68.0        | 72.0 ( $\downarrow$ 11.0) |
| DynaMo-3D [30]     | 3D-Pre-D        | PC         | 84.7        | 55.3        | 41.0        | 80.0          | 64.9 ( $\downarrow$ 11.1) | 73.0        | 76.0        | 74.5 ( $\downarrow$ 8.5)  |
| FVP [15]           | 3D-Pre-D        | PC         | 80.0        | 44.3        | 34.0        | 62.0          | 54.3 ( $\downarrow$ 21.7) | 66.0        | 76.0        | 71.0 ( $\downarrow$ 12.0) |
| DP3 [58]           | 3D-Pol          | PC         | 82.7        | 65.0        | 49.0        | 80.0          | 69.7 ( $\downarrow$ 6.3)  | 70.0        | 80.0        | 75.0 ( $\downarrow$ 8.0)  |
| <b>AFRO (Ours)</b> | <b>3D-Pre-D</b> | <b>PC</b>  | <b>88.0</b> | <b>69.7</b> | <b>55.0</b> | <b>90.7</b>   | <b>76.0</b>               | <b>82.0</b> | <b>84.0</b> | <b>83.0</b>               |

so the noisy input and condition  $(\mathbf{z}_t, \alpha_{t \rightarrow t+k}, \tau)$  flow through DiT blocks and a projector to yield  $\hat{\mathbf{z}}_{t+k}$  in one step.

**AdaLN-Zero conditioning.** Each DiT block applies identity-preserving adaptive LayerNorm  $\text{AdaLN}(\mathbf{x}; \mathbf{c}) = \text{LN}(\mathbf{x}) \odot (1 + \gamma(\mathbf{c})) + \beta(\mathbf{c})$ , with  $\mathbf{c} = \text{cond}(\mathbf{z}_t, \alpha_{t \rightarrow t+k}, \tau)$ . The scale and shift,  $\gamma(\cdot)$  and  $\beta(\cdot)$ , are produced by small MLPs and zero-initialized, keeping the residual path near identity while progressively injecting timestep and action information—enabling the one-shot denoising in Eq. (7).

### 4.3. Variance-Regularized Representation Matching

Self-supervised latent learning can easily collapse into trivial constant embeddings. To prevent this, we adopt a Variance-Invariance-Covariance Regularization (VICReg) [3] loss that preserves the statistical diversity. Given predicted features  $\hat{\mathbf{z}}$  and teacher target features  $\tilde{\mathbf{z}}$  from the EMA encoder  $f_\xi$ , the loss combines three complementary terms:

$$\mathcal{L}_{\text{VICReg}} = \lambda_I \mathcal{L}_{\text{inv}} + \lambda_V \mathcal{L}_{\text{var}} + \lambda_C \mathcal{L}_{\text{cov}}. \quad (8)$$

Here,  $\mathcal{L}_{\text{inv}}$  enforces alignment between student and teacher features,  $\mathcal{L}_{\text{var}}$  maintains sufficient variance along each dimension to avoid collapse, and  $\mathcal{L}_{\text{cov}}$  reduces cross-channel correlations for disentangled representations. Together, they stabilize latent dynamics and improve the encoder’s ability to capture coherent visual structures.

### 4.4. Pre-training Details

We train AFRO on simulated and real 3D manipulation data. The inverse dynamics module  $g_\psi$  is a 3-layer MLP with GeLU activation, outputting 16-dimensional latent actions. The forward dynamics model  $h_\theta$  is a 4-layer Transformer with adaptive conditioning. We use frame interval  $k = 4$  and train for 300 epochs using AdamW (lr=1  $\times$  10 $^{-4}$ ). The VICReg loss uses weights  $\lambda_I = \lambda_V = 25$ ,  $\lambda_C = 1$ , and sets the variance threshold  $\gamma = 1$ . The target encoder  $f_\xi$  updates via EMA with a momentum starting at 0.996.

## 5. Simulation Experiment

### 5.1. Simulation Benchmarks.

**Adroit** [38] is a high-fidelity multi-DoF anthropomorphic hand benchmark in MuJoCo focused on fine-grained control. We evaluate two tasks, *Door* and *Pen*, both of which require precise manipulation and temporal coordination.

**MetaWorld** [56] provides a diverse set of manipulation tasks using a 7-DoF Sawyer arm in MuJoCo. We select 14 representative tasks (all details in Appendix).

In MetaWorld, each task includes 25 expert trajectories generated using scripted policies, while in Adroit each task contains 100 expert trajectories produced by VRL3 [42].

### 5.2. Baseline methods.

To evaluate the effectiveness of AFRO, we compare it against four categories of baselines. (1) **End-to-End Learning** (DP3) [58] jointly learns perception and control without visual pretraining. (2) **Large-Scale Dataset Pretraining** employs visual feature extractors such as CLIP [35], DINOv2 [29], and PointNet [33] trained on large external datasets to improve generalization before diffusion policy training. (3) **Static-Only Pretraining** baselines, including Point-MAE [31] and PointDif [61], rely solely on static data, ignoring dynamic state relationships. (4) **Dynamic-Aware Pretraining** baselines, such as FVP [15], DynaMo-2D [30], and DynaMo-3D, explicitly model temporal dynamics during visual pretraining, with DynaMo-3D being our 3D extension of the original DynaMo method.

### 5.3. Implementation Details.

After visual pretraining, the encoder parameters were frozen for policy learning. We employed a diffusion policy architecture for all evaluations. Policies were trained for 100 epochs using the AdamW optimizer ( $\beta_1, \beta_2 = 0.9, 0.999$ ), a learning rate of 1e $^{-4}$  with cosine annealing, and a batch size of 128. Evaluation was conducted every 10 epochs

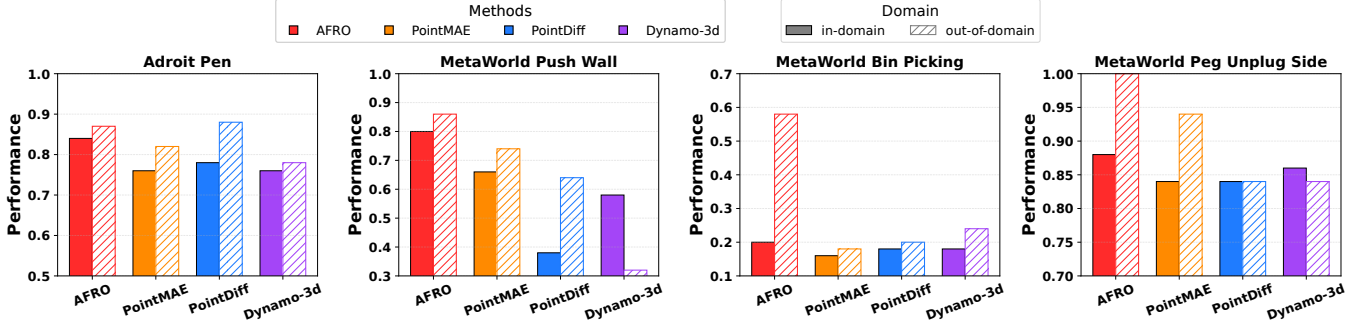


Figure 5. **Scaling across task domains.** Comparison between *in-domain* (solid) and *multi-domain* (hatched) visual pretraining on four tasks. AFRO consistently benefits from multi-domain pretraining and even reaches 100% success on *Peg Unplug Side*, whereas static and dynamic baselines show smaller or inconsistent gains.

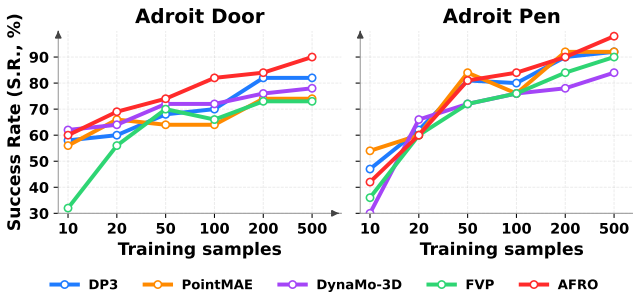


Figure 6. **Scaling with data on Adroit.** Success rate versus number of expert trajectories (10, 20, 50, 100, 200, 500) for *Door* and *Pen*.

with 25 rollouts, and we report the highest success rate among the top three performing policies. All baselines follow the same training and evaluation protocol, with experiments conducted on a single NVIDIA RTX 4090 GPU.

#### 5.4. Quantitative Results

As shown in Table 1, AFRO achieves state-of-the-art performance on both benchmarks under a unified training and evaluation protocol. Large-scale 2D models (CLIP, DINOv2) provide strong semantic priors but perform poorly on MetaWorld (24.9%, 25.9%). Among 3D methods, static approaches (PointMAE, PointDiff) benefit from geometric reconstruction yet lack temporal reasoning, while dynamic-aware baselines such as DynaMo-3D can even underperform static models. In contrast, AFRO couples diffusion-based future-feature prediction with causally structured latent-action learning, reaching **76.0%** mean success on MetaWorld (+6.3 over DP3) and **83.0%** on Adroit. The especially large gains on challenging tasks indicate that our feature differencing and inverse-consistency supervision yield stable, manipulation-oriented visual representations that better capture the causal structure of state transitions.

#### 5.5. Scalability Analysis

**Scalable Evaluation of Data.** We vary the number of expert trajectories per task  $\{10, 20, 50, 100, 200, 500\}$  on *Adroit-Door* and *Adroit-Pen* (Fig. 6). AFRO improves smoothly and dominates across all data scales. On *Door*, it reaches

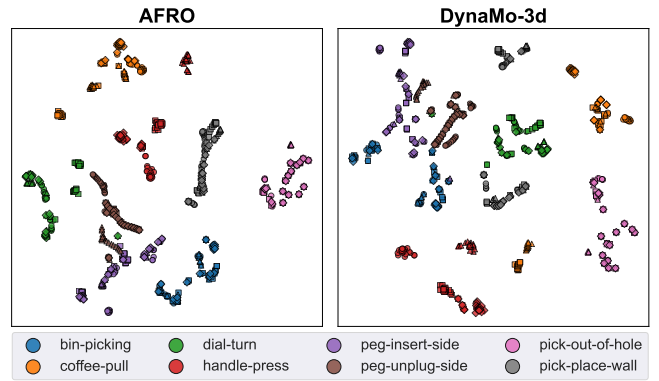


Figure 7. **t-SNE visualization of latent features on eight MetaWorld tasks.** Colors denote tasks and marker shapes denote different demonstration sequences. AFRO (left) forms clearer task clusters than DynaMo-3D (right), indicating more discriminative and temporally coherent representations.

**74%** with only 50 samples and **90%** at 500, surpassing DP3 and static pretraining baselines that plateau around 70–76%. On *Pen*, AFRO jumps from 60% to **81%** when increasing samples from 20 to 50, and further to **98%** at 500, while alternatives fluctuate or saturate early. This indicates that AFRO leverages additional data to learn richer latent dynamics, mapping unseen states to familiar transition patterns and enabling more effective policy decoding.

**Scalable Evaluation of Domain.** We evaluate how visual pretraining scales with task diversity. To this end, we conduct a multi-domain setting where the encoder is pretrained once on the union of tasks (*Door+Pen* for Adroit, all 14 tasks for MetaWorld) and then frozen while a diffusion policy is trained on the target task. As shown in Fig. 5, AFRO benefits substantially from multi-domain pretraining: average success rises from **68.0%** to **82.8%**, with *Bin Picking* improving from **20%** to **58%** and *Peg Unplug Side* reaching **100%**, whereas other methods show only modest gains or even degrade. This indicates that AFRO better exploits heterogeneous trajectories to learn transferable 3D dynamics, organizing states by transition structure rather than superficial appearance.

Table 2. **In-domain vs. out-of-domain real-world performance.** Both blocks show success rates on the same four manipulation tasks. The **blue** block uses in-domain pre-training, and the **red** block uses pre-training on a large out-of-domain dataset before task-specific fine-tuning. Orange numbers indicate the mean-success drop relative to AFRO.

| Method             | In-domain (Real-World) |           |           |           |           | Out-of-domain (Pre-train & FT) |           |           |           |           |
|--------------------|------------------------|-----------|-----------|-----------|-----------|--------------------------------|-----------|-----------|-----------|-----------|
|                    | FPP                    | BP        | CB        | B2BA      | Mean S.R. | FPP                            | BP        | CB        | B2BA      | Mean S.R. |
| DP3                | 45                     | 60        | 45        | 50        | 50 (↓ 20) | —                              | —         | —         | —         | —         |
| PointDif           | 40                     | 55        | 60        | 55        | 53 (↓ 17) | 55                             | 75        | 70        | 60        | 65 (↓ 19) |
| FVP                | 25                     | 40        | 40        | 30        | 34 (↓ 36) | 40                             | 55        | 50        | 40        | 46 (↓ 38) |
| DynaMo-3D          | 45                     | 40        | 55        | 50        | 48 (↓ 22) | 50                             | 50        | 65        | 65        | 58 (↓ 26) |
| <b>AFRO (Ours)</b> | <b>65</b>              | <b>75</b> | <b>70</b> | <b>70</b> | <b>70</b> | <b>75</b>                      | <b>90</b> | <b>85</b> | <b>85</b> | <b>84</b> |

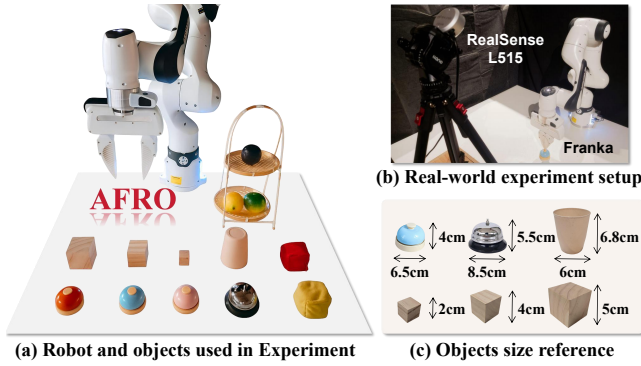


Figure 8. **Real-world evaluation setup and objects.** (a) Franka Emika arm with a parallel gripper and the objects used across tasks. (b) Physical setup with a top-down RealSense L515 RGB-D camera. (c) Size references for the main objects (dimensions in cm).

## 5.6. Representation Analysis

We visualize encoder features with t-SNE on eight Meta-World tasks after out-of-domain pre-training (Fig. 7). DynaMo-3D features are more entangled across tasks and exhibit fragmented trajectories, indicating weaker dynamic organization in latent space. In contrast, AFRO yields well-separated task clusters and smooth trajectories within each task (different marker shapes), showing both strong task discrimination and coherent temporal evolution.

## 6. Real-World Experiment

## 6.1. Experimental Setup

We evaluate on a manipulation platform built around a 7-DoF **Franka Emika** arm with a parallel gripper and a top-down **RealSense L515** depth camera; object layouts and camera/robot placement follow the real-world configuration in Fig. 8. We consider four representative manipulation tasks spanning non-prehensile and prehensile control, perception precision, and kinematic difficulty:

- **Block-to-Block Alignment:** Using non-prehensile manipulation, the robot pushes a movable block to precisely align its edge with a reference block. (*B2BA*)
  - **Bell Pressing:** The robot localizes a physical bell and presses it accurately to trigger an audible click. (*BP*)

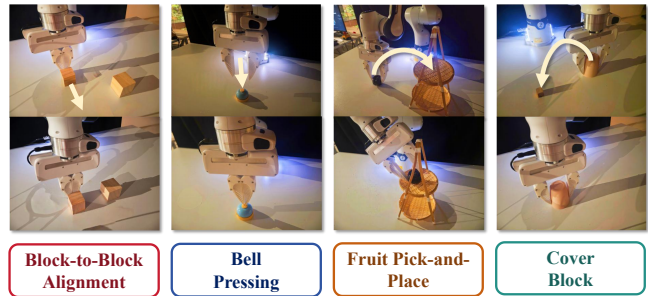


Figure 9. Demonstration of Four Tasks in Real-World.

- **Fruit Pick-and-Place:** The robot grasps a fruit from a randomized start pose and places it into a target basket. (*FPP*)
  - **Cover Block:** The robot picks up a cup from a source location, moves above a target block, and places the cup to fully cover the block. (*CB*)

For all tasks, shown in Fig. 9, object initializations are randomized within bounded perturbations to assess robustness. For each task, we collect **40 demonstrations**, and we report success rates over **20 evaluation trials**. We use a PointTransformer [59] backbone as the visual feature encoder for all real-world experiments.

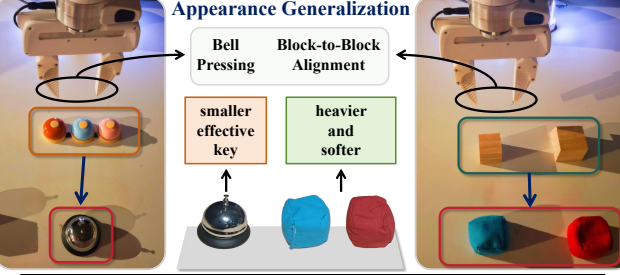
## 6.2. Real-World Task Performance

As shown in the **blue** block of Table 2, AFRO achieves the highest mean success rate of **0.70** across all four real-world tasks, outperforming DP3 (0.50), PointDif (0.53), FVP (0.34), and DynaMo-3D (0.48). The largest gains appear on *Fruit Pick-and-Place* and *Cover Block*, which involve wide-range workspace motions (e.g., lifting a fruit from the table into an elevated basket and transporting a cup over a target block). These results indicate that AFRO’s transition-centric 3D representations transfer robustly from simulation to a physical Franka setup, especially under large-magnitude spatial movements and real-world sensing noise.

### 6.3. Large-Scale Out-of-Domain Pretraining

We further evaluate scalability to large, out-of-domain data by pretraining on the RH20T [11] real-world manipulation dataset. Specifically, we construct a Franka subset (*RH20T\_Franka\_Simple*) by reconstructing point clouds from camera intrinsics and depth, cropping to a fixed

Table 3. Objects generalization performance in two tasks.



| Method             | Bell Pressing  |            | B2B Alignment  |            |
|--------------------|----------------|------------|----------------|------------|
|                    | SR (%)         | Diff ↓     | SR (%)         | Diff ↓     |
| PointDif           | 55 → 25        | <b>-30</b> | 55 → 45        | <b>-10</b> |
| FVP                | 40 → 5         | <b>-35</b> | 30 → 10        | <b>-20</b> |
| DynaMo-3d          | 40 → 15        | <b>-25</b> | 50 → 35        | <b>-15</b> |
| <b>AFRO (Ours)</b> | <b>75 → 60</b> | <b>-15</b> | <b>70 → 65</b> | <b>-5</b>  |

Table 4. Generalization Comparison: Cluttered Scenes.



| task objects       | obstacle objects |            |                |            |
|--------------------|------------------|------------|----------------|------------|
| Method             | Bell Pressing    |            | B2B Alignment  |            |
|                    | SR (%)           | Diff ↓     | SR (%)         | Diff ↓     |
| PointDif           | 55 → 40          | <b>-15</b> | 55 → 45        | <b>-10</b> |
| FVP                | 40 → 25          | <b>-15</b> | 30 → 15        | <b>-15</b> |
| DynaMo-3d          | 40 → 35          | <b>-5</b>  | 50 → 40        | <b>-10</b> |
| <b>AFRO (Ours)</b> | <b>75 → 70</b>   | <b>-5</b>  | <b>70 → 65</b> | <b>-5</b>  |

workspace, discarding the first 30 static frames, and sampling one frame every 20 from the first two scenes of over 140 tasks. On this corpus, we pretrain a shared PointTransformer encoder with **AFRO**, **DynaMo-3D**, **PointDif**, and **FVP**, then fine-tune it on four real-robot manipulation tasks with a diffusion action decoder. As shown in the red block of Table 2, AFRO benefits the most from large-scale out-of-domain pretraining, raising mean success from **70.0%** to **84%** and clearly outperforming all competing methods, indicating a stronger ability to exploit heterogeneous real-world demonstrations for transferable 3D manipulation dynamics.

#### 6.4. Generalization Evaluation

**Object Generalization.** We first evaluate how policies transfer to unseen object instances in *Bell Pressing* and *Block-to-Block Alignment*. As shown in Table 3, all baselines incur large performance drops when moving from seen to unseen objects (e.g., up to 35 points for FVP on *Bell Pressing*). In contrast, AFRO attains the highest success rates in both regimes and exhibits the smallest generalization gaps (75→60 on *BP*, 70→65 on *B2BA*), indicating that its transition-centric 3D features capture task objectives beyond object-specific appearance.

**Cluttered-Scene Generalization.** We further stress-test robustness by adding distractor objects and background clutter while keeping task definitions unchanged. Table 4 shows that all methods degrade in cluttered scenes, but AFRO remains the most stable: it drops by only 5 points on both tasks (75→70 for *Bell Pressing*, 70→65 for *B2BA*), whereas PointDif and FVP suffer notably larger losses. These results suggest that AFRO’s 3D dynamics modeling is less sensitive to spurious structures in the scene, yielding representations that generalize better across both object variation and environmental complexity.

#### 6.5. Ablation Study

As summarized in Table 5, removing any core component of AFRO consistently degrades performance on the four

Table 5. Ablation on AFRO components on real-robot tasks.

|                                                      | FPP       | BP        | CB        | B2BA      | Mean S.R.    |
|------------------------------------------------------|-----------|-----------|-----------|-----------|--------------|
| FDM: Transformer                                     | 70        | 80        | 80        | 75        | 76.25        |
| w/o $\Delta z$ Input                                 | 65        | 80        | 75        | 80        | 75.00        |
| w/o Inv. Consistency                                 | 70        | 75        | 75        | 75        | 73.75        |
| $\mathcal{L}_{VICReg} \rightarrow \mathcal{L}_{MSE}$ | 60        | 55        | 45        | 70        | 57.50        |
| $D_{act} = 64$                                       | 70        | 90        | 80        | 80        | 80.00        |
| $D_{act} = 128$                                      | 65        | 85        | 75        | 80        | 76.25        |
| Interval $k = 1$                                     | 75        | 85        | 80        | 85        | 81.25        |
| Interval $k = 16$                                    | 70        | 90        | 75        | 75        | 77.50        |
| <b>AFRO (Ours)</b>                                   | <b>75</b> | <b>90</b> | <b>85</b> | <b>85</b> | <b>84.00</b> |

real-robot tasks, confirming the necessity of our overall design. Replacing the diffusion-based forward dynamics with a deterministic transformer (*FDM: Transformer*) lowers the mean success from **84.0%** to **76.25%**, highlighting the benefit of explicitly modeling multimodal futures in latent space. Dropping feature differencing or inverse-consistency supervision (*w/o  $\Delta z$  Input*, *w/o Inv. Consistency*) causes further drops, indicating that learning latent actions from representation changes and enforcing bidirectional consistency are both important to prevent feature leakage and stabilize training. Switching the pretraining objective from the variance-regularized VICReg loss to a plain MSE on features ( $\mathcal{L}_{VICReg} \rightarrow \mathcal{L}_{MSE}$ ) leads to a large collapse in mean success (**57.50%**), confirming that latent feature learning is prone to collapse without constraints on the feature distribution. Varying the latent action dimension ( $D_{act} = 64, 128$ ) and the temporal interval used for frame sampling in pre-training (*Interval  $k = 1, 16$* , vs. our default  $k = 4$ ) yields intermediate performance that never surpasses AFRO, suggesting that our chosen latent capacity and moderate frame interval strike a favorable balance between expressiveness and temporal coverage in practice.

## 7. Conclusion

We introduced AFRO, an action-free 3D visual pre-training framework that learns dynamics-aware, manipulation-relevant representations in latent space by combining latent actions with diffusion-based forward dynamics, achieving strong performance and generalization on simulated and real-world manipulation tasks. Free from action labels, AFRO naturally scales to large unlabeled 3D robot interaction data, including data generated in simulation. A natural next step is to fuse AFRO with semantic priors from visual foundation models, targeting 3D representations that are both dynamics-aware and semantically grounded, further broadening open-world manipulation capabilities.

## References

- [1] Arthur Allshire, Roberto Martín-Martín, Charles Lin, Shawn Manuel, Silvio Savarese, and Animesh Garg. Laser: Learning a latent action space for efficient reinforcement learning. In *2021 IEEE International Conference on Robotics and Automation (ICRA)*, pages 6650–6656. IEEE, 2021. 3
- [2] Mido Assran, Adrien Bardes, David Fan, Quentin Garrido, Russell Howes, Matthew Muckley, Ammar Rizvi, Claire Roberts, Koustuv Sinha, Artem Zholus, et al. V-jepa 2: Self-supervised video models enable understanding, prediction and planning. *arXiv preprint arXiv:2506.09985*, 2025. 2
- [3] Adrien Bardes, Jean Ponce, and Yann LeCun. Vi-creg: Variance-invariance-covariance regularization for self-supervised learning. *arXiv preprint arXiv:2105.04906*, 2021. 2, 5
- [4] Qingwen Bu, Yanting Yang, Jisong Cai, Shenyuan Gao, Guanghui Ren, Maoqing Yao, Ping Luo, and Hongyang Li. Univla: Learning to act anywhere with task-centric latent actions. *arXiv preprint arXiv:2505.06111*, 2025. 2, 3
- [5] Shizhe Chen, Ricardo Garcia, Ivan Laptev, and Cordelia Schmid. Sugar: Pre-training 3d visual representations for robotics. In *Proceedings of the IEEE/CVF Conference on Computer Vision and Pattern Recognition (CVPR)*, pages 18049–18060, 2024. 2
- [6] Xiaoyu Chen, Hangxing Wei, Pushi Zhang, Chuheng Zhang, Kaixin Wang, Yanjiang Guo, Rushuai Yang, Yucen Wang, Xinquan Xiao, Li Zhao, et al. Villa-x: enhancing latent action modeling in vision-language-action models. *arXiv preprint arXiv:2507.23682*, 2025. 3
- [7] Cheng Chi, Zhenjia Xu, Siyuan Feng, Eric Cousineau, Yilun Du, Benjamin Burchfiel, Russ Tedrake, and Shuran Song. Diffusion policy: Visuomotor policy learning via action diffusion. *The International Journal of Robotics Research*, 44(10-11):1684–1704, 2025. 12
- [8] Jeremy A Collins, Loránd Cheng, Kunal Aneja, Albert Wilcox, Benjamin Joffe, and Animesh Garg. Amplify: Actionless motion priors for robot learning from videos. *arXiv preprint arXiv:2506.14198*, 2025. 3
- [9] Sudeep Dasari, Mohan Kumar Srirama, Unnat Jain, and Abhinav Gupta. An unbiased look at datasets for visuo-motor pre-training. In *Conference on Robot Learning (CoRL)*, pages 1183–1198. PMLR, 2023. 1
- [10] Zibin Dong, Fei Ni, Yifu Yuan, Yinchuan Li, and Jianye Hao. Embodiedmae: A unified 3d multi-modal representation for robot manipulation. *arXiv preprint arXiv:2505.10105*, 2025. 2
- [11] Hao-Shu Fang, Hongjie Fang, Zhenyu Tang, Jirong Liu, Chenxi Wang, Junbo Wang, Haoyi Zhu, and Cewu Lu. Rh20t: A comprehensive robotic dataset for learning diverse skills in one-shot. *arXiv preprint arXiv:2307.00595*, 2023. 2, 7, 13
- [12] Shenyuan Gao, Siyuan Zhou, Yilun Du, Jun Zhang, and Chuang Gan. Adaworld: Learning adaptable world models with latent actions. *arXiv preprint arXiv:2503.18938*, 2025. 3
- [13] Theophile Gervet, Zhou Xian, Nikolaos Gkanatsios, and Katerina Fragkiadaki. Act3d: 3d feature field transformers for multi-task robotic manipulation. *arXiv preprint arXiv:2306.17817*, 2023. 12
- [14] Ankit Goyal, Jie Xu, Yijie Guo, Valts Blukis, Yu-Wei Chao, and Dieter Fox. Rvt: Robotic view transformer for 3d object manipulation. In *Conference on Robot Learning (CoRL)*, pages 694–710. PMLR, 2023. 1, 12
- [15] Chengkai Hou, Yanjie Ze, Yankai Fu, Zeyu Gao, Songbo Hu, Yue Yu, Shanghang Zhang, and Huazhe Xu. 4d visual pre-training for robot learning. In *Proceedings of the IEEE/CVF International Conference on Computer Vision (ICCV)*, pages 8451–8461, 2025. 3, 5
- [16] Jialei Huang, Shuo Wang, Fanqi Lin, Yihang Hu, Chuan Wen, and Yang Gao. Tactile-vla: Unlocking vision-language-action model’s physical knowledge for tactile generalization. *arXiv preprint arXiv:2507.09160*, 2025. 12
- [17] Siyuan Huang, Yichen Xie, Song-Chun Zhu, and Yixin Zhu. Spatio-temporal self-supervised representation learning for 3d point clouds. In *Proceedings of the IEEE/CVF international conference on computer vision (ICCV)*, pages 6535–6545, 2021. 2
- [18] Yueru Jia, Jiaming Liu, Sixiang Chen, Chenyang Gu, Zhilue Wang, Longzan Luo, Lily Lee, Pengwei Wang, Zhongyuan Wang, Renrui Zhang, et al. Lift3d foundation policy: Lifting 2d large-scale pretrained models for robust 3d robotic manipulation. *arXiv preprint arXiv:2411.18623*, 2024. 2
- [19] Guangqi Jiang, Yifei Sun, Tao Huang, Huanyu Li, Yongyuan Liang, and Huazhe Xu. Robots pre-train robots: Manipulation-centric robotic representation from large-scale robot datasets. *arXiv preprint arXiv:2410.22325*, 2024. 1
- [20] Ya Jing, Xuelin Zhu, Xingbin Liu, Qie Sima, Taozheng Yang, Yunhai Feng, and Tao Kong. Exploring visual pre-training for robot manipulation: Datasets, models and methods. In *2023 IEEE/RSJ International Conference on Intelligent Robots and Systems (IROS)*, pages 11390–11395, 2023. 1
- [21] Gagan Khandate, Boxuan Wang, Sarah Park, Weizhe Ni, Joaquin Palacios, Kathryn Lampo, Philippe Wu, Rosh Ho, Eric Chang, and Matei Ciocarlie. Train robots in a jif: Joint inverse and forward dynamics with human and robot demonstrations. *arXiv preprint arXiv:2503.12297*, 2025. 3
- [22] Moo Jin Kim, Karl Pertsch, Siddharth Karamcheti, Ted Xiao, Ashwin Balakrishna, Suraj Nair, Rafael Rafailov, Ethan Foster, Grace Lam, Pannag Sanketi, et al. Openvla: An open-source vision-language-action model. *arXiv preprint arXiv:2406.09246*, 2024. 12
- [23] Seungjae Lee, Yibin Wang, Haritheja Etukuru, H Jin Kim, Nur Muhammad Mahi Shafiqullah, and Lerrel Pinto. Behavior generation with latent actions. *arXiv preprint arXiv:2403.03181*, 2024. 3

- [24] Anthony Liang, Pavel Czempin, Matthew Hong, Yutai Zhou, Erdem Biyik, and Stephen Tu. Clam: Continuous latent action models for robot learning from unlabeled demonstrations. *arXiv preprint arXiv:2505.04999*, 2025. 3
- [25] Qiwei Liang, Boyang Cai, Rongyi He, Hui Li, Tao Teng, Haohan Duan, Changxin Huang, and Runhao Zeng. Whole-body coordination for dynamic object grasping with legged manipulators. *arXiv preprint arXiv:2508.08328*, 2025. 1
- [26] Yecheng Jason Ma, Shagun Sodhani, Dinesh Jayaraman, Ossert Bastani, Vikash Kumar, and Amy Zhang. Vip: Towards universal visual reward and representation via value-implicit pre-training. In *The Eleventh International Conference on Learning Representations (ICLR)*, 2023. 1, 2
- [27] Suraj Nair, Aravind Rajeswaran, Vikash Kumar, Chelsea Finn, and Abhinav Gupta. R3m: A universal visual representation for robot manipulation. In *Conference on Robot Learning (CoRL)*, pages 892–909. PMLR, 2023. 1, 2
- [28] Alexander Nikulin, Ilya Zisman, Denis Tarasov, Nikita Lyubaykin, Andrei Polubarov, Igor Kiselev, and Vladislav Kurenkov. Latent action learning requires supervision in the presence of distractors. *arXiv preprint arXiv:2502.00379*, 2025. 3
- [29] Maxime Oquab, Timothée Darcet, Théo Moutakanni, Huy Vo, Marc Szafraniec, Vasil Khalidov, Pierre Fernandez, Daniel Haziza, Francisco Massa, Alaaeldin El-Nouby, et al. Dinov2: Learning robust visual features without supervision. *arXiv preprint arXiv:2304.07193*, 2023. 5
- [30] Maxime Oquab, Timothée Darcet, Théo Moutakanni, Huy Vo, Marc Szafraniec, Vasil Khalidov, Pierre Fernandez, Daniel Haziza, Francisco Massa, Alaaeldin El-Nouby, et al. Dinov2: Learning robust visual features without supervision. *Transactions on Machine Learning Research Journal*, pages 1–31, 2024. 3, 5
- [31] Yatian Pang, Wenxiao Wang, Francis EH Tay, Wei Liu, Yonghong Tian, and Li Yuan. Masked autoencoders for point cloud self-supervised learning. In *European Conference on Computer Vision (ECCV)*, pages 604–621, 2022. 5
- [32] William Peebles and Saining Xie. Scalable diffusion models with transformers. In *Proceedings of the IEEE/CVF international conference on computer vision*, pages 4195–4205, 2023. 4
- [33] Charles R Qi, Hao Su, Kaichun Mo, and Leonidas J Guibas. Pointnet: Deep learning on point sets for 3d classification and segmentation. In *Proceedings of the IEEE conference on computer vision and pattern recognition (CVPR)*, pages 652–660, 2017. 2, 5
- [34] Shengyi Qian, Kaichun Mo, Valts Blukis, David F Fouhey, Dieter Fox, and Ankit Goyal. 3d-mvp: 3d multiview pretraining for manipulation. In *Proceedings of the Computer Vision and Pattern Recognition Conference (CVPR)*, pages 22530–22539, 2025. 2
- [35] Alec Radford, Jong Wook Kim, Chris Hallacy, Aditya Ramesh, Gabriel Goh, Sandhini Agarwal, Girish Sastry, Amanda Askell, Pamela Mishkin, Jack Clark, et al. Learning transferable visual models from natural language supervision. In *International conference on machine learning (ICML)*, pages 8748–8763. PMLR, 2021. 5
- [36] Ilija Radosavovic, Baifeng Shi, Letian Fu, Ken Goldberg, Trevor Darrell, and Jitendra Malik. Robot learning with sensorimotor pre-training. In *Conference on Robot Learning (CoRL)*, pages 683–693. PMLR, 2023. 1
- [37] Ilija Radosavovic, Tete Xiao, Stephen James, Pieter Abbeel, Jitendra Malik, and Trevor Darrell. Real-world robot learning with masked visual pre-training. In *Conference on Robot Learning (CoRL)*, pages 416–426. PMLR, 2023. 1
- [38] Aravind Rajeswaran, Vikash Kumar, Abhishek Gupta, Giulia Vezzani, John Schulman, Emanuel Todorov, and Sergey Levine. Learning complex dexterous manipulation with deep reinforcement learning and demonstrations. In *Robotics: Science and Systems (RSS)*, 2018. 5
- [39] Mohit Shridhar, Lucas Manuelli, and Dieter Fox. Perceiver-actor: A multi-task transformer for robotic manipulation. In *Conference on Robot Learning*, pages 785–799. PMLR, 2023. 12
- [40] Mohan Kumar Srirama, Sudeep Dasari, Shikhar Bahl, and Abhinav Gupta. Hrp: Human affordances for robotic pre-training. *arXiv preprint arXiv:2407.18911*, 2024. 1
- [41] Bahey Tharwat, Yara Nasser, Ali Abouzeid, and Ian Reid. Latent action pretraining through world modeling. *arXiv preprint arXiv:2509.18428*, 2025. 3
- [42] Che Wang, Xufang Luo, Keith Ross, and Dongsheng Li. Vrl3: A data-driven framework for visual deep reinforcement learning. *Advances in Neural Information Processing Systems (NeurIPS)*, 35:32974–32988, 2022. 5
- [43] Jianyuan Wang, Minghao Chen, Nikita Karaev, Andrea Vedaldi, Christian Rupprecht, and David Novotny. Vggt: Visual geometry grounded transformer. In *Proceedings of the Computer Vision and Pattern Recognition Conference*, pages 5294–5306, 2025. 14
- [44] Taowen Wang, Cheng Han, James Liang, Wenhao Yang, Dongfang Liu, Luna Xinyu Zhang, Qifan Wang, Jiebo Luo, and Ruixiang Tang. Exploring the adversarial vulnerabilities of vision-language-action models in robotics. In *Proceedings of the IEEE/CVF International Conference on Computer Vision (ICCV)*, pages 6948–6958, 2025. 12
- [45] Zijian Wang and Mac Schwager. Kinematic multi-robot manipulation with no communication using force feedback. In *2016 IEEE international conference on robotics and automation (ICRA)*, pages 427–432. IEEE, 2016. 12
- [46] Kun Wu, Chengkai Hou, Jiaming Liu, Zhengping Che, Xiaozhu Ju, Zhuqin Yang, Meng Li, Yinuo Zhao, Zhiyuan Xu, Guang Yang, et al. Robomind: Benchmark on multi-embodiment intelligence normative data for robot manipulation. *arXiv preprint arXiv:2412.13877*, 2024. 2
- [47] Qiwei Wu, Xuanbin Peng, Jiayu Zhou, Zhuoran Sun, Xiaogang Xiong, and Yunjiang Lou. Rttf: Rapid tactile transfer framework for contact-rich manipulation tasks. In *2024 IEEE/RSJ International Conference on Intelligent Robots and Systems (IROS)*, pages 2913–2920. IEEE, 2024. 12
- [48] Qiwei Wu, Haidong Wang, Jiayu Zhou, Xiaogang Xiong, and Yunjiang Lou. Tars: Tactile affordance in robot synesthesia for dexterous manipulation. *IEEE Robotics and Automation Letters*, 2024. 12
- [49] Tete Xiao, Ilija Radosavovic, Trevor Darrell, and Jitendra Malik. Masked visual pre-training for motor control. *arXiv preprint arXiv:2203.06173*, 2022. 1, 2
- [50] Saining Xie, Jiatao Gu, Demi Guo, Charles R Qi, Leonidas Guibas, and Or Litany. Pointcontrast: Unsupervised pre-training for 3d point cloud understanding. In *European conference on computer vision (ECCV)*, pages 574–591. Springer, 2020. 2

- [51] Lixin Xu, Zixuan Liu, Zhewei Gui, Jingxiang Guo, Zeyu Jiang, Zhixuan Xu, Chongkai Gao, and Lin Shao. Dexsin-grasp: Learning a unified policy for dexterous object simulation and grasping in cluttered environments. *arXiv preprint arXiv:2504.04516*, 2025. 12
- [52] Dejie Yang, Zijing Zhao, and Yang Liu. Ar-vrm: Imitating human motions for visual robot manipulation with analogical reasoning. In *Proceedings of the IEEE/CVF International Conference on Computer Vision (ICCV)*, pages 6818–6827, 2025. 2
- [53] Jiange Yang, Yansong Shi, Haoyi Zhu, Mingyu Liu, Kaijing Ma, Yating Wang, Gangshan Wu, Tong He, and Limin Wang. Como: Learning continuous latent motion from internet videos for scalable robot learning. *arXiv preprint arXiv:2505.17006*, 2025. 3
- [54] Seonghyeon Ye, Joel Jang, Byeongguk Jeon, Sejune Joo, Jianwei Yang, Baolin Peng, Ajay Mandlekar, Reuben Tan, Yu-Wei Chao, Bill Yuchen Lin, et al. Latent action pretraining from videos. *arXiv preprint arXiv:2410.11758*, 2024. 3
- [55] Lin Yen-Chen, Andy Zeng, Shuran Song, Phillip Isola, and Tsung-Yi Lin. Learning to see before learning to act: Visual pre-training for manipulation. In *2020 IEEE International Conference on Robotics and Automation (ICRA)*, pages 7286–7293. IEEE, 2020. 1
- [56] Tianhe Yu, Deirdre Quillen, Zhanpeng He, Ryan Julian, Karol Hausman, Chelsea Finn, and Sergey Levine. Meta-world: A benchmark and evaluation for multi-task and meta reinforcement learning. In *Conference on robot learning (CoRL)*, pages 1094–1100. PMLR, 2020. 5
- [57] Xumin Yu, Lulu Tang, Yongming Rao, Tiejun Huang, Jie Zhou, and Jiwen Lu. Point-bert: Pre-training 3d point cloud transformers with masked point modeling. In *Proceedings of the IEEE/CVF conference on computer vision and pattern recognition (CVPR)*, pages 19313–19322, 2022. 2
- [58] Yanjie Ze, Gu Zhang, Kangning Zhang, Chenyuan Hu, Muhan Wang, and Huazhe Xu. 3d diffusion policy: Generalizable visuomotor policy learning via simple 3d representations. In *2nd Workshop on Dexterous Manipulation: Design, Perception and Control (RSS)*, 2024. 5
- [59] Hengshuang Zhao, Li Jiang, Jiaya Jia, Philip HS Torr, and Vladlen Koltun. Point transformer. In *Proceedings of the IEEE/CVF international conference on computer vision ICCV*, pages 16259–16268, 2021. 7
- [60] Ruijie Zheng, Xiyao Wang, Yanchao Sun, Shuang Ma, Jieyu Zhao, Huazhe Xu, Hal Daumé III, and Furong Huang. TACO: Temporal latent action-driven contrastive loss for visual reinforcement learning. *Advances in Neural Information Processing Systems*, 36:48203–48225, 2023. 3
- [61] Xiao Zheng, Xiaoshui Huang, Guofeng Mei, Yuenan Hou, Zhaoyang Lyu, Bo Dai, Wanli Ouyang, and Yongshun Gong. Point cloud pre-training with diffusion models. In *Proceedings of the IEEE/CVF Conference on Computer Vision and Pattern Recognition (CVPR)*, pages 22935–22945, 2024. 5
- [62] Yuhang Zheng, Xiangyu Chen, Yupeng Zheng, Songen Gu, Runyi Yang, Bu Jin, Pengfei Li, Chengliang Zhong, Zengmao Wang, Lina Liu, et al. Gaussiangrasper: 3d language gaussian splatting for open-vocabulary robotic grasping. *IEEE Robotics and Automation Letters*, 2024. 12
- [63] Jiayu Zhou, Qiwei Wu, Jian Li, Zhe Chen, Xiaogang Xiong, and Renjing Xu. Gentle manipulation policy learning via demonstrations from vlm planned atomic skills. *arXiv preprint arXiv:2511.05855*, 2025. 12
- [64] Wenxuan Zhou, Sujay Bajracharya, and David Held. Plas: Latent action space for offline reinforcement learning. In *Conference on Robot Learning (CoRL)*, pages 1719–1735. PMLR, 2021. 3
- [65] Haoyi Zhu, Yating Wang, Di Huang, Weicai Ye, Wanli Ouyang, and Tong He. Point cloud matters: Rethinking the impact of different observation spaces on robot learning. *Advances in Neural Information Processing Systems*, 37:77799–77830, 2024. 1

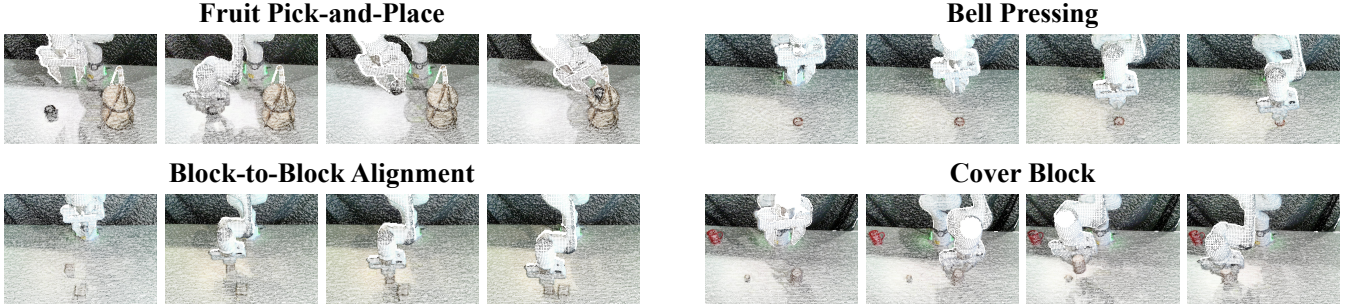


**Figure 10. Point-cloud rollouts for four real-world tasks.** We visualize the 3D point clouds captured by the top-down RealSense L515 depth camera for four representative manipulation tasks on the Franka platform: Fruit Pick-and-Place, Bell Pressing, Block-to-Block Alignment, and Cover Block (from left to right and top to bottom). Each block shows four temporally ordered point clouds from a successful AFRO rollout, illustrating the evolution from the initial configuration, through approach and contact, to task completion. Across tasks, the manipulated objects (fruit and basket, bell, blocks, cup and target block) undergo large spatial motion while the surrounding table and robot geometry remain largely static. These visualizations highlight that AFRO is trained directly on such raw point clouds and must learn dynamics-aware representations that are sensitive to object motion and interaction, yet robust to background clutter and viewpoint changes.

## A. Abstract

In this appendix, we complement the main paper with additional analyses and results for AFRO. We first situate our approach within the broader literature on robotic manipulation. We then provide qualitative visualizations of AFRO rollouts on four real-world Franka tasks using point-cloud observations, as well as the complete per-task results on all Adroit and MetaWorld benchmarks. Next, we describe in more detail how we process the large-scale RH20T dataset to obtain point-cloud inputs for pre-training. Finally, we discuss current limitations of AFRO and outline several promising directions for scaling, enriching semantics, incorporating multi-view dynamics, and improving latent-space learning objectives.

## B. Additional Related Work

### B.1. Robotics Manipulation.

Robotic manipulation aims to transform object states in the physical world, from basic grasping [51, 62] to long-horizon, contact-rich [47] tasks. Early systems decomposed perception, grasp planning, and motion planning, while recent work learns end-to-end policies from rich sensory inputs such as RGB(-D) [7], tactile [16, 48, 63], and force feedback [45], often with additional safety constraints [44] or language conditioning. Vision–language–action models [22] further condition policies on natural-language goals but are still mostly built on 2D image encoders, which struggle with occlusions and precise 6-DoF reasoning. To overcome these limitations, recent approaches use 3D-aware policies that operate on depth, multi-view RGB-D, or point clouds, such as methods that infer volumetric features or explicit 3D action maps [13, 14, 39]. Our work is complementary: instead of introducing another policy head, AFRO provides a 3D dynamics-aware representation that can be plugged into existing diffusion-based manipulation policies with minimal changes.

## C. Additional Real-World Visualizations

The main paper evaluates AFRO on four real-robot tasks that span non-prehensile pushing, precise contact interaction, and long-horizon pick-and-place motions using a Franka Emika arm and a top-down depth sensor. In Fruit Pick-and-Place, the robot must reach for a fruit at a randomized pose and place it into a distant basket; in Bell Pressing, it must localize a small bell and press it with sufficient accuracy to trigger the mechanism; in Block-to-Block Alignment, it pushes a movable block until its edge is aligned with a fixed reference block; and in Cover Block, it lifts a cup and places it so that the cup fully covers a target block. In all cases, object positions and orientations are randomized within bounded ranges to test robustness.

Figure 10 provides additional qualitative insight into how these tasks appear in the point-cloud observation space. For each task we render four representative frames, showing the pre-contact configuration, the approach of the end-effector, the main interaction phase (pressing, pushing, or grasping), and the final configuration after successful completion. The sequences illustrate the substantial 3D motion, self-occlusion, and depth noise present in real scenes, as well as the diversity of object geometries (e.g., thin bell handle versus bulky fruit or cup). AFRO is pre-trained and fine-tuned directly on such sequences, and the strong real-world performance reported in the main paper indicates that its latent dynamics modeling can extract task-relevant structure from these raw point-cloud trajectories.

## D. Complete MetaWorld Results

Table 6 reports per-task success rates on all 16 simulated manipulation tasks used in our study: two Adroit hand tasks (Door, Pen) and fourteen MetaWorld tasks spanning four difficulty levels (Easy, Medium, Hard, Very Hard). For each method, we train a diffusion policy on top of the corresponding visual encoder using 100 expert trajectories for each Adroit task and 25 trajectories for each MetaWorld task, and

Table 6. **Comparison across 16 simulated manipulation tasks.** Success rates (%) for AFRO and competing methods on two Adroit tasks and fourteen MetaWorld tasks grouped by difficulty. Best results are highlighted in red, and second-best results are highlighted in orange. All methods use the same diffusion-policy architecture and training protocol: policies are trained from 100 expert trajectories on Adroit and 25 trajectories on each MetaWorld task, and evaluated over 50 rollouts every 10 epochs; we report the best success rate over multiple runs.

| Method             | Adroit    |           | MetaWorld (Easy) |              |                 |             | MetaWorld (Medium) |                 |  |
|--------------------|-----------|-----------|------------------|--------------|-----------------|-------------|--------------------|-----------------|--|
|                    | Door      | Pen       | Dial Turn        | Handle Press | Peg Unplug Side | Bin Picking | Coffee Pull        | Peg Insert Side |  |
| CILP               | 61        | 84        | 0                | 88           | 0               | 0           | 72                 | 0               |  |
| DINOv2             | 76        | 84        | 6                | 90           | 6               | 0           | 58                 | 0               |  |
| PointNet           | 80        | 72        | 56               | 90           | 68              | 62          | 66                 | 54              |  |
| PointMAE           | 64        | 76        | 60               | 88           | 84              | 16          | 94                 | 82              |  |
| PointDif           | 76        | 78        | 76               | 90           | 84              | 18          | 90                 | 84              |  |
| Dynamo             | 76        | 68        | 18               | 84           | 24              | 18          | 34                 | 14              |  |
| Dynamo-3D          | 73        | 76        | 70               | 98           | 86              | 18          | 68                 | 76              |  |
| FVP                | 66        | 76        | 72               | 88           | 80              | 16          | 66                 | 70              |  |
| DP3                | 70        | 80        | 76               | 86           | 86              | 18          | 90                 | 74              |  |
| <b>AFRO (Ours)</b> | <b>82</b> | <b>84</b> | <b>78</b>        | <b>98</b>    | <b>88</b>       | <b>20</b>   | <b>92</b>          | <b>92</b>       |  |

| Method             | MetaWorld (Medium) |           |           | MetaWorld (Hard) |           | MetaWorld (Very Hard) |            |                 |
|--------------------|--------------------|-----------|-----------|------------------|-----------|-----------------------|------------|-----------------|
|                    | Push Wall          | Soccer    | Sweep     | Pick Out of Hole | Push      | Stick Pull            | Stick Push | Pick Place Wall |
| CILP               | 6                  | 0         | 6         | 0                | 10        | 66                    | 100        | 0               |
| DINOv2             | 2                  | 24        | 0         | 0                | 10        | 66                    | 100        | 0               |
| PointNet           | 40                 | 24        | 52        | 10               | 36        | 30                    | 88         | 48              |
| PointMAE           | 66                 | 22        | 88        | 16               | 68        | 58                    | 76         | 76              |
| PointDif           | 38                 | 26        | 92        | 20               | 62        | 52                    | 76         | 48              |
| Dynamo             | 26                 | 26        | 12        | 16               | 12        | 16                    | 72         | 14              |
| Dynamo-3D          | 58                 | 24        | 88        | 4                | 78        | 60                    | 100        | 80              |
| FVP                | 36                 | 34        | 44        | 26               | 42        | 24                    | 84         | 78              |
| DP3                | 78                 | 38        | 92        | 24               | 74        | 58                    | 88         | 94              |
| <b>AFRO (Ours)</b> | <b>80</b>          | <b>36</b> | <b>98</b> | <b>32</b>        | <b>78</b> | <b>78</b>             | <b>100</b> | <b>94</b>       |

evaluate success over 50 rollouts every 10 epochs; the table shows the best success rate over multiple runs under this shared protocol. Compared to all baselines, AFRO attains the highest mean performance and achieves the best result on the majority of tasks, ranking second only on Bin Picking, Coffee Pull, and Soccer. These fine-grained results complement the aggregated comparisons in the main paper and confirm that AFRO consistently improves over both 2D and 3D pre-training baselines across a broad range of contact-rich skills.

## E. Further Details on RH20T

RH20T[11] (Robot–Human demonstration in 20TB) is a large-scale, real-world robotic manipulation dataset designed to support one-shot imitation learning and general skill learning across diverse, contact-rich tasks. The dataset contains over 110,000 robot manipulation sequences paired with an equal number of human demonstration videos, resulting in more than 50 million image frames in total and about 20 TB of data. It demonstrates over 140 different tasks, including a wide variety of operational tasks. Each robot sequence is recorded in the real world and includes synchronized multi-modal information such as RGB and depth im-

ages, force/torque measurements, audio, and low-level robot state and action signals, together with a corresponding human demonstration video and a language description for the same skill. We generate a point cloud for each frame by back-projecting the depth map into 3D space using the corresponding camera intrinsics. We then apply farthest point sampling (FPS) to downsample the raw point cloud to 1024 points. Empirically, we find that 1024 points provide sufficient geometric coverage to capture the object contours while at the same time substantially reducing the computational cost of the PointTransformer encoder.

## F. Limitations and Future Work

Although AFRO achieves strong performance across diverse simulated and real-world manipulation tasks, several limitations remain.:contentReference[oaicite:0]index=0 First, our current pre-training regime is moderate in scale compared with truly large vision foundation models: we use task-specific simulation data and a subset of RH20T rather than hundreds of millions of frames. Second, the objective is predominantly dynamics-driven. While this helps encode transition structure, the learned features still lack the rich semantic coverage that large 2D or 3D visual models obtain

from web-scale data. Third, our framework is instantiated with single-view point clouds from a fixed depth camera; it does not yet exploit the multi-view nature of real 3D environments, such as fusing observations from multiple cameras over time. Fourth, the latent action is an abstract variable optimized only for predictive performance; it does not have explicit physical meaning (e.g., end-effector displacement, velocity, or contact force), which limits its interpretability and potential reuse. Finally, AFRO relies on VICReg-style variance regularization to prevent collapse in latent space; as shown in our ablations, removing this constraint severely harms performance, indicating that training stability is still tied to a relatively strong handcrafted objective.

These observations suggest several directions for future work. (1) **Scaling and semantic grounding.** We plan to combine AFRO with strong semantic backbones such as VGGT [43] or DINOv2 style models, either by distilling their features into the 3D encoder or by joint multi-task pre-training. This would aim to obtain representations that are simultaneously dynamics-aware and semantically rich. (2) **Larger-scale pre-training.** A natural extension is to train AFRO on substantially larger and more diverse 3D robot datasets, including multi-embodiment, multi-task, and web-scale synthetic data, to approach the scale of general-purpose visual foundation models for robotics. (3) **Multi-view 3D dynamics.** Incorporating multi-view inputs and explicitly modeling cross-view consistency of dynamics (e.g., by fusing trajectories from several cameras) could make the representation more robust to occlusion and viewpoint changes and better suited to mobile manipulation. (4) **Physically grounded latent actions.** We are interested in tying latent actions to physically interpretable quantities, for example by supervising them with estimated optical flow, 3D scene flow, or end-effector trajectories, so that the latent space captures meaningful motion primitives that can be reused across tasks and robots. (5) **Collapse-free objectives beyond VICReg.** Finally, we aim to explore alternative self-supervised objectives—such as JEPA-style prediction, information-theoretic regularization, or architectural constraints—that maintain feature diversity without relying on explicit variance penalties, potentially simplifying training and further improving robustness of the learned 3D representations.